Comparative study on equivalent models calculating magnetic force between permanent magnets

Yuyang Zhang and Yonggang Leng
School of Mechanical Engineering, Tianjin University, Tianjin, China and Key Laboratory of Mechanism Theory and Equipment Design of Ministry of Education, Tianjin, China
Hao Zhang
UK-China Joint Special Equipment and Robot Intelligence Research Center, London, UK, and
Xukun Su, Shuailing Sun, Xiaoyu Chen and Junjie Xu
School of Mechanical Engineering, Tianjin University, Tianjin, China and Key Laboratory of Mechanism Theory and Equipment Design of Ministry of Education, Tianjin, China

Received 22 September 2020
Revised 9 October 2020
Accepted 9 October 2020

Abstract

Purpose – An appropriate equivalent model is the key to the effective analysis of the system and structure in which permanent magnet takes part. At present, there are several equivalent models for calculating the interacting magnetic force between permanent magnets including magnetizing current, magnetic charge and magnetic dipole–dipole model. How to choose the most appropriate and efficient model still needs further discussion.

Design/methodology/approach – This paper chooses cuboid, cylindrical and spherical permanent magnets as calculating objects to investigate the detailed calculation procedures based on three equivalent models, magnetizing current, magnetic charge and magnetic dipole–dipole model. By comparing the accuracies of those models with experiment measurement, the applicability of three equivalent models for describing permanent magnets with different shapes is analyzed.

Findings – Similar calculation accuracies of the equivalent magnetizing current model and magnetic charge model are verified by comparison between simulation and experiment results. However, the magnetic dipole–dipole model can only accurately calculate for spherical magnet instead of other nonellipsoid magnets, because dipole model cannot describe the specific characteristics of magnet's shape, only sphere can be treated as the topological form of a dipole, namely a filled dot.

Originality/value – This work provides reference basis for choosing a proper model to calculate magnetic force in the design of electromechanical structures with permanent magnets. The applicability of different equivalent models describing permanent magnets with different shapes is discussed and the equivalence between the models is also analyzed.

Keywords Permanent magnet, Magnetic force calculation, Equivalent magnetizing current, Equivalent magnetic charge, Magnetic dipole

Paper type Research paper

This work is supported by the National Natural Science Foundation of China (grant No. 51675370) and the National key R&D projects of China (grant No. 2018YFD0700704).

Journal of Intelligent Manufacturing and Special Equipment
Vol. 1 No. 1, 2020
pp. 43-65
Emerald Publishing Limited
e-ISSN: 2633-660X
p-ISSN: 2633-6596
DOI 10.1108/JIMSE-09-2020-0009

1. Introduction

Interaction between permanent magnets is popularly used in many fields such as electromechanical system, industrial robots, magnetic machineries, vibration energy harvesters and some other frontier researches, because of its special character such as nonlinearity and noncontact (Gysen *et al.*, 2010; Zhang *et al.*, 2017a; Kim *et al.*, 2016; Teyber *et al.*, 2017). An increasing number of researchers has devoted themselves in the characteristics of interaction between permanent magnets (Wang *et al.*, 2012; Liu *et al.*, 2009; Hutterer *et al.*, 2017; Kim and Choi, 2016). Therefore, accurate magnetic force calculation is the key to effectively design and analyze the performance and property of a system in which permanent magnet takes part.

At present, there are several calculation methods of interacting magnetic force between permanent magnets. Magnetic force calculation based on equivalent models is more understandable and acceptable, used in the design and analysis of mechanical engineering. Equivalent model describing magnet is a classical hot research topic (Choi *et al.*, 2006; Liang *et al.*, 2016; Li, 2018; Janssen *et al.*, 2010; Zhao *et al.*, 2015; Sun *et al.*, 2016; Liu *et al.*, 2006). Among several equivalent models proposed before such as magnetic charge, magnetizing current and magnetic dipole model, how to choose the most appropriate and efficient equivalent model for different permanent magnets still requires further discussion.

The most common shapes of permanent magnet used in mechanical structures are cuboid, cylinder and sphere (Wang, 2007; Zhao, 2003). Permanent magnet with excessive complicated shape is not liable to be utilized and controlled, especially in active control, vibration energy harvesting system. In this paper, we fully calculate the interacting magnetic force based on equivalent magnetic dipole, charge and magnetizing current model, respectively. We set up the experiment using cuboid, cylindrical and spherical permanent magnets as measuring objects to verify the accuracies of each model. The mathematical modeling processes of interacting magnetic force are demonstrated in detail. Besides, we analyze the applicability of each model and equivalency among these models by comparison.

2. Magnetic force calculation

2.1 Equivalent magnetizing current model

In modern electromagnetic theory, the equivalent magnetization current model believes that each magnetic moment can be equivalently regarded as a small circular current, namely molecular current. An unmagnetized permanent magnet does not show external magnetism due to the chaotic distribution of internal magnetic moments. Whereas the internal micro-current rings of permanent magnet turn in one direction due to the external magnetized magnetic field, as shown in Figure 1 (Zhao and Chen, 2011). In the case of a uniformly magnetized spherical permanent magnet whose magnetization intensity M is constant, the internal adjacent magnetizing ring currents have inverse tangential directions and are offset by each other. Thus, only the outmost surface of the permanent magnet has magnetic currents around it.

The internal magnetizing current density is $\boldsymbol{J}_m = \nabla \times \boldsymbol{M} = 0$, and the surface magnetizing current density is $\boldsymbol{K}_m = \boldsymbol{M} \times \hat{\boldsymbol{n}}$, where $\hat{\boldsymbol{n}}$ is surface normal unit vector.

Therefore, the interaction between permanent magnets is equivalent to the interaction between current loops. Magnetic induction intensity generated by a permanent magnet in space can be calculated according to Biot–Savart's law. The magnetic induction intensity generated by a section of current element at arbitrary point P in space can be expressed as:

$$\boldsymbol{B} = \int_L \frac{\mu_0 I}{4\pi} \frac{d\boldsymbol{l} \times \boldsymbol{r}}{r^3}, \tag{1}$$

where $I = \int_t K_m dt$, t represents the width of the current, L is the integral path of the current, dl represents the unit current element, r is the vector pointing to the P from the current element and μ_0 is the space permeability.

Similarly, the force acting on the permanent magnet in external magnetic field is equivalent to the ampere force on the surface magnetizing current:

$$\boldsymbol{F} = \iint_S \boldsymbol{K}_m \times \boldsymbol{B} ds, \tag{2}$$

where S represents the area of the surface where the current flows (Agashe *et al.*, 2008; Bobbio and Delfino, 2000).

2.1.1 Cuboid permanent magnet. The Cartesian coordinate system is established as shown in Figure 2 on the account of the flat surfaces and straight lines of cuboid permanent magnet. The current flows in the negative direction along the x-axis, $\boldsymbol{R}$ represents the vector pointing to arbitrary point $P(x, y, z)$ in the space from the origin of coordinates. We have the following relations:

$$\boldsymbol{R} = x\boldsymbol{i} + y\boldsymbol{j} + z\boldsymbol{k} \tag{3}$$

$$\boldsymbol{l} = w\boldsymbol{i},\ d\boldsymbol{l} = -dw\boldsymbol{i} \tag{4}$$

$$\boldsymbol{r} = \boldsymbol{R} - \boldsymbol{l} = (x - w)\boldsymbol{i} + y\boldsymbol{j} + z\boldsymbol{k} \tag{5}$$

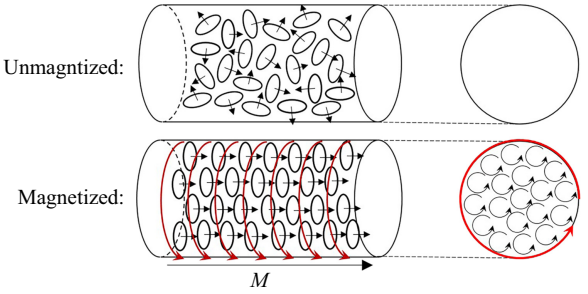

Figure 1.
Schematic drawing of equivalent magnetizing current model of permanent magnet (Zhao and Chen, 2011)

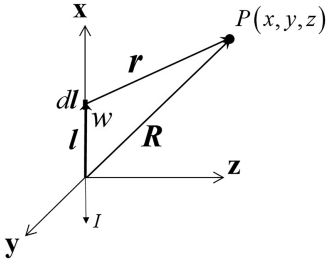

Figure 2.
Coordinate system of magnetic field produced by a current

$$d\boldsymbol{l}\times\boldsymbol{r}=\begin{vmatrix}\boldsymbol{i} & \boldsymbol{j} & \boldsymbol{k}\\ -dw & 0 & 0\\ x-w & y & z\end{vmatrix}=zdw\boldsymbol{j}-ydw\boldsymbol{k} \tag{6}$$

$$r=\left[(x-w)^2+y^2+z^2\right]^{1/2} \tag{7}$$

For the convenient calculation, the geometric center of the cuboid permanent magnet is selected as the origin point of coordinate system. After simple coordinate transformation, the coordinate system is established as shown in Figure 3, where the magnetization direction of the permanent magnet A is alone the z axis. The equivalent magnetization current distribution can be determined according to the right-hand screw rule and the surface current is expressed as $\boldsymbol{I}=\int \boldsymbol{K}_{mA}dt=\int_{-l_B/2}^{l_B/2}\boldsymbol{M}_A\times\hat{\boldsymbol{n}}dt$.

l_A, w_A and h_A marked in Figure 3 represent the length, width and height of permanent magnet A, respectively. The surface magnetizing current of cuboid permanent magnet can be divided into four parts, and the magnetic induction intensity is the sum of the action of top, bottom, front and back surface magnetizing current of permanent magnet. Thus, the magnetic induction intensities produced by cuboid magnet A in x, y and z directions respectively are:

$$B_i(x,y,z)=\frac{\mu_0 M_A}{4\pi}\int_{-\frac{l_A}{2}}^{\frac{l_A}{2}}dz_1\left\{\int_{-\frac{w_A}{2}}^{\frac{w_A}{2}}\frac{(z-z_1)dw_1}{\left[\left(x-\frac{h_A}{2}\right)^2+(y-w_1)^2+(z-z_1)^2\right]^{\frac{3}{2}}}\right.$$
$$\left.+\int_{-\frac{w_B}{2}}^{\frac{w_B}{2}}\frac{-(z-z_1)dw_1}{\left[\left(x+\frac{h_A}{2}\right)^2+(y-w_1)^2+(z-z_1)^2\right]^{\frac{3}{2}}}\right\} \tag{8}$$

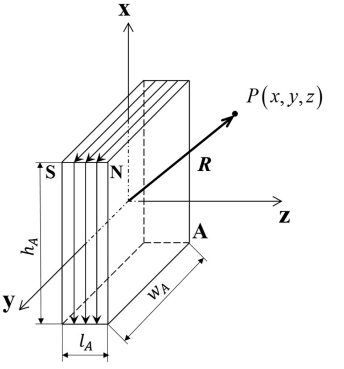

Figure 3.
Schematic diagram of magnet A's magnetizing currents

$$B_j(x,y,z)=\frac{\mu_0 M_A}{4\pi}\int_{-\frac{l_A}{2}}^{\frac{l_A}{2}}dz_1\left\{\int_{-\frac{w_A}{2}}^{\frac{w_A}{2}}\frac{(z-z_1)dh_1}{\left[(x-h_1)^2+\left(y-\frac{w_A}{2}\right)^2+(z-z_1)^2\right]^{\frac{3}{2}}}\right.$$
$$\left.+\int_{-\frac{w_B}{2}}^{\frac{w_B}{2}}\frac{-(z-z_1)dh_1}{\left[(x-h_1)^2+\left(y+\frac{w_A}{2}\right)^2+(z-z_1)^2\right]^{\frac{3}{2}}}\right\} \tag{9}$$

$$B_k(x,y,z)=\frac{\mu_0 M_A}{4\pi}\int_{-\frac{l_A}{2}}^{\frac{l_A}{2}}dz_1\left\{\int_{-\frac{h_A}{2}}^{\frac{h_A}{2}}\frac{-\left(y-\frac{w_A}{2}\right)dh_1}{\left[(x-h_1)^2+\left(y-\frac{w_A}{2}\right)^2+(z-z_1)^2\right]^{\frac{3}{2}}}\right.$$
$$+\int_{-\frac{h_A}{2}}^{\frac{h_A}{2}}\frac{\left(y+\frac{w_A}{2}\right)dh_1}{\left[(x-h_1)^2+\left(y+\frac{w_A}{2}\right)^2+(z-z_1)^2\right]^{\frac{3}{2}}}$$
$$+\int_{-\frac{w_A}{2}}^{\frac{w_A}{2}}\frac{\left(x+\frac{h_A}{2}\right)dw_1}{\left[\left(x+\frac{h_A}{2}\right)^2+(y-w_1)^2+(z-z_1)^2\right]^{\frac{3}{2}}}$$
$$\left.+\int_{-\frac{w_A}{2}}^{\frac{w_A}{2}}\frac{-\left(x-\frac{h_A}{2}\right)dw_1}{\left[\left(x-\frac{h_A}{2}\right)^2+(y-w_1)^2+(z-z_1)^2\right]^{\frac{3}{2}}}\right\} \tag{10}$$

If another same permanent magnet B is placed in such an external field $\boldsymbol{B}=[B_i\ B_j\ B_k]$ we achieved, the acted magnetic force is equivalent to the ampere force acted on the surface magnetizing current of magnet B. The length, width and height of permanent magnets B are respectively expressed as l_B, w_B and h_B, as shown in Figure 4. Here, the like magnetic poles are arranged face to face, which means the axial repulsive magnetic forces exist between the magnet pair in our case.

Figure 4 shows the position of the surface equivalent magnetizing currents of permanent magnet B in the coordinate system. The coordinates of the center points on the top, bottom, front and back surfaces of permanent magnet B are respectively: $K_{m1}\left(x+\frac{h_B}{2},y,z\right)$, $K_{m2}\left(x-\frac{h_B}{2},y,z\right)$, $K_{m3}\left(x,y+\frac{w_B}{2},z\right)$ and $K_{m4}\left(x,y-\frac{w_B}{2},z\right)$, where (x,y,z) is the coordinate

of the geometric center point of magnet B, which represents the relative position of permanent magnet B in the magnetic field generated by permanent magnet A. The relation $z = d + \frac{l_A}{2} + \frac{l_B}{2}$ can be obtained, where d is the axial interval between two magnets.

Based on the definition of the equivalent surface magnetization current density $\boldsymbol{K}_m = \boldsymbol{M} \times \hat{\boldsymbol{n}}$, the magnetization current density on each side of permanent magnet B can be written as:

$$\begin{bmatrix} \boldsymbol{K}_{m1} \\ \boldsymbol{K}_{m2} \\ \boldsymbol{K}_{m3} \\ \boldsymbol{K}_{m4} \end{bmatrix} = \begin{bmatrix} -M_B \boldsymbol{j} \\ M_B \boldsymbol{j} \\ M_B \boldsymbol{i} \\ -M_B \boldsymbol{i} \end{bmatrix}. \tag{11}$$

Therefore, the interaction magnetic force between two cuboid permanent magnets A and B can be derived from Eqn (2):

$$\begin{aligned} \boldsymbol{F}(x, y, z) = & \int_{-l_2/2}^{l_2/2} \left[- \int_{-\frac{w_B}{2}}^{\frac{w_B}{2}} M_B B_k \left(x + \frac{h_B}{2}, y + w_2, z + z_2 \right) dw_2 \right. \\ & \left. + \int_{-\frac{w_B}{2}}^{\frac{w_B}{2}} M_B B_k \left(x - \frac{h_B}{2}, y + w_2, z + z_2 \right) dw_2 \right] dz_2 \boldsymbol{i} \\ & + \int_{-l_2/2}^{l_2/2} \left[- \int_{-\frac{h_B}{2}}^{\frac{h_B}{2}} M_B B_k \left(x + h_2, y + \frac{w_B}{2}, z + z_2 \right) dh_2 \right. \\ & \left. + \int_{-\frac{h_B}{2}}^{\frac{h_B}{2}} M_B B_k \left(x + h_2, y - \frac{w_B}{2}, z + z_2 \right) dh_2 \right] dz_2 \boldsymbol{j} \\ & + \int_{-l_2/2}^{l_2/2} \left[+ \int_{-\frac{w_B}{2}}^{\frac{w_B}{2}} M_B B_i \left(x + \frac{h_B}{2}, y + w_2, z + z_2 \right) dw_2 \right. \\ & - \int_{-\frac{w_B}{2}}^{\frac{w_B}{2}} M_B B_i \left(x - \frac{h_B}{2}, y + w_2, z + z_2 \right) dw_2 \\ & + \int_{-\frac{h_B}{2}}^{\frac{h_B}{2}} M_B B_j \left(x + h_2, y + \frac{w_B}{2}, z + z_2 \right) dh_2 \\ & \left. - \int_{-\frac{h_B}{2}}^{\frac{h_B}{2}} M_B B_j \left(x + h_2, y - \frac{w_B}{2}, z + z_2 \right) dh_2 \right] dz_2 \boldsymbol{k} \end{aligned} \tag{12}$$

2.1.2 Cylindrical permanent magnet. For an axially magnetized cylindrical permanent magnet, the distribution of surface equivalent magnetization current is circular around

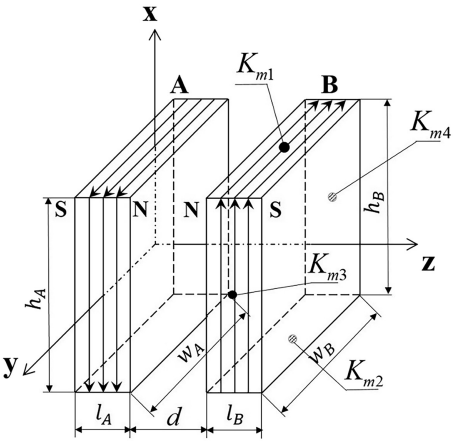

Figure 4.
The positions of magnetizing currents on the surfaces of interacting magnets in the coordinate system

magnetization axis. Therefore, we need to first analyze the magnetic induction intensity generated by a circular current. Referring to the calculation method of the straight line current in Section 2.1.1, the coordinate system is established taking the center of the circle current as the original point shown in Figure 5. The following relations can be achieved:

$$\boldsymbol{R} = x\boldsymbol{i} + y\boldsymbol{j} + z\boldsymbol{k}, \tag{13}$$

$$l = l\cos\theta\boldsymbol{i} + l\sin\theta\boldsymbol{j},\ d\boldsymbol{l} = -l\sin\theta\, d\theta\boldsymbol{i} + l\cos\theta\, d\theta\boldsymbol{j}, \tag{14}$$

$$\boldsymbol{r} = \boldsymbol{R} - \boldsymbol{l} = (x - l\cos\theta)\boldsymbol{i} + (y - l\sin\theta)\boldsymbol{j} + z\boldsymbol{k}, \tag{15}$$

$$d\boldsymbol{l}\times\boldsymbol{r} = zl\cos\theta\, d\theta\boldsymbol{i} + zl\sin\theta\, d\theta\boldsymbol{j} + l(l - x\cos\theta - y\sin\theta)d\theta\boldsymbol{k}. \tag{16}$$

Subsequently, we move the origin of coordinate system to the geometric center of cylindrical magnet A. The magnetic induction intensity at arbitrary point $P(x,y,z)$ produced by cylindrical magnet A can be derived as:

$$\boldsymbol{B} = \frac{\mu_0 M_A}{4\pi}\int_{-l_A/2}^{l_A/2} dz_1 \int_0^{2\pi}\left(\frac{(z-z_1)r_A\cos\theta}{r^3}d\theta\boldsymbol{i} + \frac{(z-z_1)r_A\sin\theta}{r^3}d\theta\boldsymbol{j}\right.$$
$$\left. + \frac{r_A(r_A - x\cos\theta - y\sin\theta)}{r^3}d\theta\boldsymbol{k}\right), \tag{17}$$

where $r = \left((x - r_A\cos\theta)^2 + (y - r_A\sin\theta)^2 + (z - z_1)^2\right)^{1/2}$, l_A and r_A denote the thickness and radius of cylindrical magnet A, respectively.

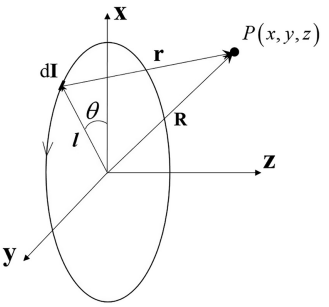

Figure 5.
Coordinate system of magnetic field produced by a circular current loop

Similarly, the force on a cylindrical permanent magnet B in the external magnetic field is calculated by using the Ampere's law. The interacting magnetic force between two same cylindrical permanent magnets is as follows:

$$\boldsymbol{F} = \iint_S \boldsymbol{K}_{mB} \times \boldsymbol{B} dS = \iint_S \begin{vmatrix} \boldsymbol{i} & \boldsymbol{j} & \boldsymbol{k} \\ -M_B \sin\varphi & M_B \cos\varphi & 0 \\ B_i & B_j & B_k \end{vmatrix} dz_2 r_B d\varphi, \tag{18}$$

where $\begin{bmatrix} B_i \\ B_j \\ B_k \end{bmatrix} = \begin{bmatrix} B_i(x + r_B\cos\varphi,\, y + r_B\sin\varphi,\, z + z_2) \\ B_j(x + r_B\cos\varphi,\, y + r_B\sin\varphi,\, z + z_2) \\ B_k(x + r_B\cos\varphi,\, y + r_B\sin\varphi,\, z + z_2) \end{bmatrix}$. Hence, the interacting magnetic force between two cylindrical permanent magnets is derived:

$$\begin{aligned} \boldsymbol{F} = & \left[M_B \int_{-l_B/2}^{l_B/2} dz_2 \int_0^{2\pi} B_k(x + r_B\cos\varphi,\, y + r_B\sin\varphi,\, z + z_2)\cos\varphi r_B d\varphi \right] \boldsymbol{i} \\ & + \left[M_B \int_{-l_B/2}^{l_B/2} dz_2 \int_0^{2\pi} B_k(x + r_B\cos\varphi,\, y + r_B\sin\varphi,\, z + z_2)\sin\varphi r_B d\varphi \right] \boldsymbol{j} \\ & - \left[M_B \int_{-l_B/2}^{l_B/2} dz_2 \int_0^{2\pi} B_i(x + r_B\cos\varphi,\, y + r_B\sin\varphi,\, z + z_2)\cos\varphi r_B d\varphi \right. \\ & \left. + M_B \int_{-l_B/2}^{l_B/2} dz_2 \int_0^{2\pi} B_j(x + r_B\cos\varphi,\, y + r_B\sin\varphi,\, z + z_2)\sin\varphi r_B d\varphi \right] \boldsymbol{k} \end{aligned} \tag{19}$$

where $z = d + \frac{l_A}{2} + \frac{l_B}{2}$, l_B and r_B are thickness and radius of cylindrical magnet B, respectively. Coordinates (x, y, z) represent the center position of cylindrical magnet B, as shown in Figure 6.

2.1.3 Spherical permanent magnet. For spherical permanent magnet magnetized along one diameter direction, the surface equivalent magnetization current is still circular. However, due to 3D curved surface of sphere in every direction, diameters of the current loops change with different positions, interaction of spherical permanent magnet is also calculated by summing interactions of the magnetizing current loops.

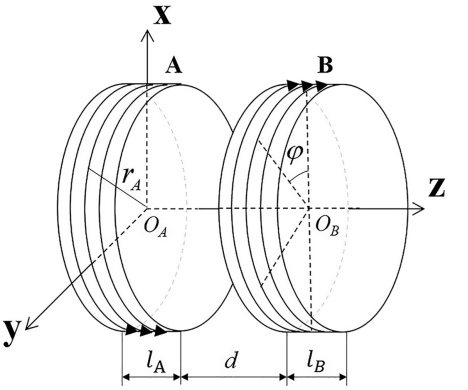

Figure 6.
The positions of magnetizing currents on the surface of cylindrical magnets in the coordinate system

The calculation process of spherical permanent magnet is similar to that of other shapes. For convenience, the center of the sphere is taken as the origin of coordinates, Cartesian coordinate system is established taking the direction of magnetization as the z-axis, as shown in Figure 7(a). It is noteworthy that the distribution of surface magnetizing current of spherical permanent magnets is not uniform, which is different from that of cuboid and cylindrical permanent magnets. According to the definition of equivalent magnetizing surface current density $\boldsymbol{K}_m = \boldsymbol{M}\times\hat{\boldsymbol{n}} = M\sin\varphi$, the current at different positions on the surface is respect to the angle φ. Based on the calculation method of magnetic induction intensity generated by circular current as shown in Figure 5 in Section 2.1.2, the magnetic induction intensity generated by spherical permanent magnet A at arbitrary point in space is achieved:

$$\boldsymbol{B} = \frac{\mu_0 M_A}{4\pi}\int_0^{\pi} R_A\sin\varphi d\varphi \int_0^{2\pi}\left(\frac{(z-R_A\cos\varphi)R_A\sin\varphi\cos\alpha}{r^3}d\alpha\boldsymbol{i} + \frac{(z-R_A\cos\varphi)R_A\sin\varphi\sin\alpha}{r^3}d\alpha\boldsymbol{j} - \frac{R_A\sin\varphi(R_A\sin\varphi - x\cos\alpha - y\sin\alpha)}{r^3}d\alpha\boldsymbol{k}\right), \tag{20}$$

where $r = \begin{pmatrix}(x-R_A\sin\varphi\cos\alpha)^2\\ +(y-R_A\sin\varphi\sin\alpha)^2\\ +(z-R_A\cos\varphi)^2\end{pmatrix}^{1/2}$, R_A is the radius of spherical magnet A.

Another spherical permanent magnet B is acted in given external magnetic field $[B_i \quad B_j \quad B_k]$, as shown in Figure 7(b). The acted force can be derived as:

$$\begin{aligned}\boldsymbol{F} &= \iint_S \boldsymbol{K}_{mB}\times\boldsymbol{B}dS = \iint_S (\boldsymbol{M}_B\times\hat{\boldsymbol{n}})\times\boldsymbol{B}dS\\ &= \iint_S \begin{vmatrix}\boldsymbol{i} & \boldsymbol{j} & \boldsymbol{k}\\ M_B R_B\sin\theta\sin\beta d\beta & -M_B R_B\sin\theta\cos\beta d\beta & 0\\ B_i(x',y',z') & B_j(x',y',z') & B_k(x',y',z')\end{vmatrix} R_B\sin\theta d\theta,\end{aligned} \tag{21}$$

where $\begin{bmatrix}x'\\ y'\\ z'\end{bmatrix} = \begin{bmatrix}x+R_B\sin\theta\cos\beta\\ y+R_B\sin\theta\sin\beta\\ z+R_B\cos\theta\end{bmatrix}$ represents coordinate of each current element, (x,y,z) is the coordinate of center of sphere B. R_A and R_B denotes radiuses of spherical magnet, M_A and M_B represent intensities of magnetization.

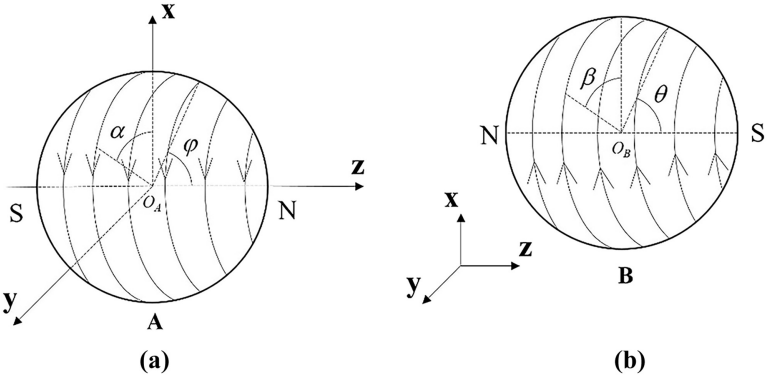

Figure 7.
The positions of surface magnetizing currents on spherical permanent magnet in coordinate system. (a) producing magnetic field, (b) acted magnetic force

2.2 Magnetic charge model

The equivalent magnetic charge theory is based on the magnetic dipole model as its micro model. One magnetic moment is equivalent to one magnetic dipole composed of a pair of opposite (one positive and one negative) magnetic charges. For permanent magnet with macro volume, it states that the magnetic charges gather in the surfaces of magnetic poles. An unmagnetized permanent magnet has no magnetism at macro scale, because the magnetic dipolar molecules are random in the magnet. For a magnetized permanent magnet, the internal magnetic moments are arranged along the direction of the external magnetic field, where the positive and negative charges are orderly linked. It means that positive and negative magnetic charges only distribute on the surfaces of magnetic north and south poles, the internal charges are offset by each other, as shown in Figure 8 (Zan, 2008). The interaction between permanent magnets can be equivalent to the interaction of these magnetic charges on the surfaces.

The equivalent magnetic charge model of permanent magnet is obtained in comparison with Coulomb interaction of electrical charges. The interacting magnetic force between a pair of magnetic charges is similar to that of electric charges $\boldsymbol{F} = K\frac{q_1 q_2}{r^2}\widehat{\boldsymbol{r}}$, where q_1 and q_2 represent the elementary point magnetization charges, $\widehat{r}$ is a unit vector of the vector $\boldsymbol{r}$ linking two charges and K is a coefficient $K = \frac{1}{4\pi\mu_0}$, where μ_0 is permeability of vacuum (Li, 2015).

2.2.1 Cuboid permanent magnet. Before we calculate the interaction between permanent magnets, we first need to analyze the interaction between two magnetic pole faces, where magnetic charges uniformly distribute. We use a coordinate system as shown in Figure 9 with its origin located at the middle point of pole face 1, belonging to one cuboid magnet's north pole, on which positive magnetic charges distribute uniformly. The interacting magnetic force between these two square planes can be calculated by using twice surface integrals:

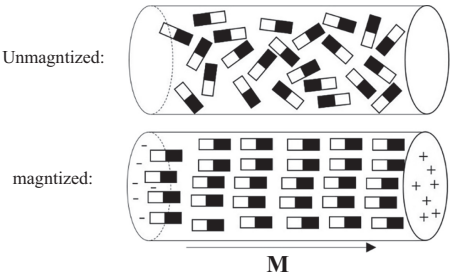

Figure 8.
Schematic drawing of equivalent magnetic charge model of permanent magnet

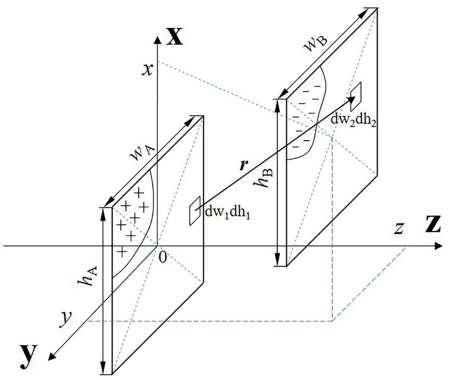

Figure 9.
Coordinate system of the interaction between two unlike magnetic pole faces where magnetic charges distribute

$$\boldsymbol{F}(x, y, z) = \int_{S_1}\int_{S_2}\frac{p_{m1}p_{m2}}{4\pi\mu_0 r^3}\boldsymbol{r}, \tag{22}$$

where $p_{m1} = \sigma_{sA}dh_1dw_1$, and $p_{m2} = \sigma_{sB}dh_2dw_2$. A permanent magnet, equivalent to a model of accumulated magnetic charges, is composed of a volume charge density $\sigma_v = -\mu_0 div\boldsymbol{M}$ and a surface charge density $\sigma_s = \mu_0(\boldsymbol{n}\cdot\boldsymbol{M})$. The volume charge density is zero for a magnet magnetized uniformly with a constant $\boldsymbol{M}$ and the surface charge densities are given by $\sigma_{sA} = \mu_0 M_A$ and $\sigma_{sB} = \mu_0 M_B$ (Sadowski *et al.*, 1992). The detailed expression of interacting force between two square magnetic pole faces covered with positive or negative magnetic charges shown in Figure 9 has the following form:

$$\begin{aligned}\boldsymbol{F}_{mn}(x, y, z) =& \pm\frac{\sigma_{sA}\sigma_{sB}}{4\pi\mu_0}\int_{-\frac{h_A}{2}}^{\frac{h_A}{2}}\int_{-\frac{w_A}{2}}^{\frac{w_A}{2}}\int_{-\frac{h_B}{2}}^{\frac{h_B}{2}}\int_{-\frac{w_B}{2}}^{\frac{w_B}{2}}\frac{(x+h_2-h_1)dw_1dh_1dw_2dh_2}{\left((x+h_2-h_1)^2+(y+w_2-w_1)^2+z^2\right)^{3/2}}\boldsymbol{i}\\ &\pm\frac{\sigma_{sA}\sigma_{sB}}{4\pi\mu_0}\int_{-\frac{h_A}{2}}^{\frac{h_A}{2}}\int_{-\frac{w_A}{2}}^{\frac{w_A}{2}}\int_{-\frac{h_B}{2}}^{\frac{h_B}{2}}\int_{-\frac{w_B}{2}}^{\frac{w_B}{2}}\frac{(y+w_2-w_1)dw_1dh_1dw_2dh_2}{\left((x+h_2-h_1)^2+(y+w_2-w_1)^2+z^2\right)^{3/2}}\boldsymbol{j}\\ &\pm\frac{\sigma_{sA}\sigma_{sB}}{4\pi\mu_0}\int_{-\frac{h_A}{2}}^{\frac{h_A}{2}}\int_{-\frac{w_A}{2}}^{\frac{w_A}{2}}\int_{-\frac{h_B}{2}}^{\frac{h_B}{2}}\int_{-\frac{w_B}{2}}^{\frac{w_B}{2}}\frac{zdw_1dh_1dw_2dh_2}{\left((x+h_2-h_1)^2+(y+w_2-w_1)^2+z^2\right)^{3/2}}\boldsymbol{k}\end{aligned} \tag{23}$$

where h_A, h_B, w_A and w_B in Eqn (2) denote the heights and widths of two square magnetic pole faces; d is the interval between the magnets; l_A and l_B denote the thicknesses of magnets, as shown in Figure 10. The magnets are placed in the way that their poles are faced to each other. Hence, the interacting force between cuboid magnets is a sum of the contribution from both magnetic poles faces of two permanent magnets.

$$\boldsymbol{F} = \boldsymbol{F}_{23}(x, y, d) + \boldsymbol{F}_{14}(x, y, d + l_A + l_B) - \boldsymbol{F}_{13}(x, y, d + l_B) - \boldsymbol{F}_{24}(x, y, d + l_A). \tag{24}$$

2.2.2 Cylindrical permanent magnet. For a pair of cylindrical magnets, the basic theory of equivalent magnetic charge is the same as that of aforementioned cuboid magnets.

We transform the Cartesian coordinate system to a cylindrical coordinate system as shown in Figure 11. Similar to cuboid magnet's force, the axial and lateral interacted magnetic forces F_{Zmn} and F_{Lmn} between two circular magnetic pole faces covered with positive or negative magnetic charges are also obtained by using twice surface integrals,

$$\begin{aligned}F_{Zmn}(z, L) =& \pm\int_0^{r_B}\int_0^{2\pi}\int_0^{r_A}\int_0^{2\pi}\frac{\sigma_{S1}\sigma_{S2}r_1r_2}{4\pi\mu_0}\frac{z}{\left(\begin{array}{l}(L+r_2\cos\beta-r_1\cos\alpha)^2\\ +(r_2\sin\beta-r_1\sin\alpha)^2+z^2\end{array}\right)^{3/2}}d\beta dr_1 d\alpha dr_2\\ F_{Lmn}(z, L) =& \pm\int_0^{r_B}\int_0^{2\pi}\int_0^{r_A}\int_0^{2\pi}\frac{\sigma_{S1}\sigma_{S2}r_1r_2}{4\pi\mu_0}\frac{(L+r_2\cos\beta-r_1\cos\alpha)}{\left(\begin{array}{l}(L+r_2\cos\beta-r_1\cos\alpha)^2\\ +(r_2\sin\beta-r_1\sin\alpha)^2+z^2\end{array}\right)^{3/2}}d\beta dr_1 d\alpha dr_2\end{aligned} \tag{25}$$

where the indications of parameters r_1, α, r_2 and β are shown in Figure 11. The interacting magnetic force between two cylindrical permanent magnets is the sum of the contribution from both circular magnetic pole faces, that is,

$$\begin{aligned} F_Z &= F_{Z23}(d, r) + F_{Z14}(d + l_A + l_B, r) - F_{Z13}(d + l_B, r) - F_{Z24}(d + l_A, r) \\ F_L &= F_{L23}(d, r) + F_{L14}(d + l_A + l_B, r) - F_{L13}(d + l_B, r) - F_{L24}(d + l_A, r), \end{aligned} \tag{26}$$

where d is the interval between magnets; l_A and l_B denote the thicknesses of magnets, as shown in Figure 12. F_Z and F_L represent the axial and lateral magnet forces between permanent cylindrical magnets, respectively.

2.2.3 Spherical permanent magnet. Since the surface of the spherical permanent magnet is continuous spherical surface, it is necessary to transform the plane integral into the spherical integral by using trigonometric relations.

We define the serial number for every hemispherical surface in Figure 13, the interacting force between two spherical permanent magnets is a summation of the contribution of both hemispherical magnetic pole surfaces of two permanent magnets:

$$\boldsymbol{F} = \sum_{m=1}^{2} \sum_{n=3}^{4} \boldsymbol{F}_{mn} \tag{27}$$

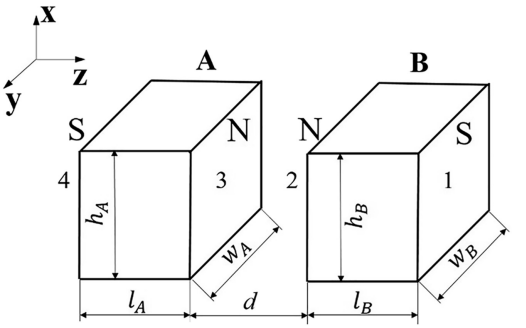

Figure 10.
Schematic diagram of geometric dimensions and interval between two cuboid magnets

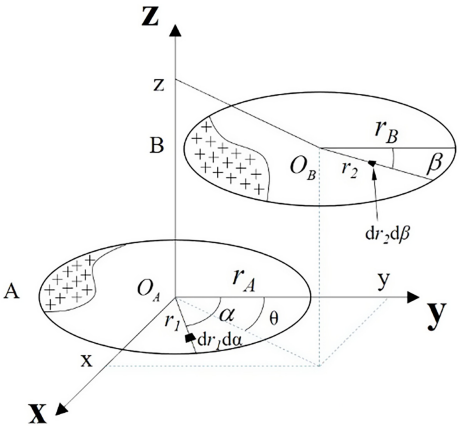

Figure 11.
Coordinate system of interacting circular magnetic pole faces

where F_{mn} represents the interacting magnetic force between two hemispherical surfaces, which belongs to different magnet:

$$\boldsymbol{F}_{mn} = \int_0^{\pi/2}\int_0^{2\pi}\int_0^{\pi/2}\int_0^{2\pi} \frac{R_A^2 R_B^2 \sin\varphi\sin\theta\cos\varphi\cos\theta d\varphi d\theta d\alpha d\beta (x + R_A\sin\theta\cos\beta - R_B\sin\varphi\cos\alpha)}{r^{3/2}} \boldsymbol{i} + \int_0^{\pi/2}\int_0^{2\pi}\int_0^{\pi/2}\int_0^{2\pi} \frac{R_A^2 R_B^2 \sin\varphi\sin\theta\cos\varphi\cos\theta d\varphi d\theta d\alpha d\beta z_{mn}}{r^{3/2}} \boldsymbol{k}, \tag{28}$$

where $r = [(x + R_A\sin\theta\cos\beta - R_B\sin\varphi\cos\alpha)^2 + (R_A\sin\theta\sin\beta - R_B\sin\varphi\sin\alpha)^2 + z_{mn}]$.

The parameters α, β, φ and θ are shown in Figure 13, R is the radius of spherical magnet. The z_{mn} in this equation is used to distinguish the interaction between different pairs of hemispherical surfaces numbered in Figure 13 and these are:

$$z_{23} = d + R_B(1 - \cos\varphi) + R_A(1 - \cos\theta), \tag{29}$$

$$z_{13} = d + R_B(1 - \cos\varphi) + R_A(1 + \cos\theta), \tag{30}$$

$$z_{24} = d + R_B(1 + \cos\varphi) + R_A(1 - \cos\theta), \tag{31}$$

$$z_{14} = d + R_B(1 + \cos\varphi) + R_A(1 + \cos\theta). \tag{32}$$

For z_{13} and z_{24}, the signs in the front of Eqn (28) are minus, for z_{14} and z_{23}, the signs are plus similar to the definition in electric charge model.

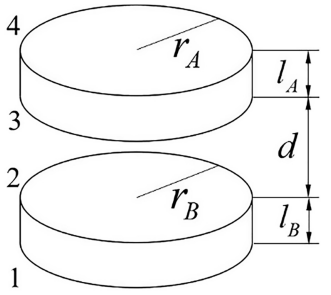

Figure 12.
Schematic diagram of geometric dimensions and interval between two cylindrical magnets

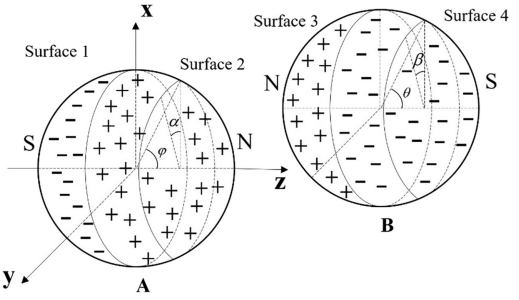

Figure 13.
The positions of surface magnetic charges of spherical permanent magnets in coordinate system

2.3 Magnetic dipole–dipole model

The theory of magnetic dipole–dipole treats two interacting permanent magnets as a pair of magnetic dipoles with directional magnetic moments $\boldsymbol{m} = \boldsymbol{M}V$, where $\boldsymbol{M}$ is the magnetization intensity of permanent magnet and V represents the volume of magnet. The magnetic induction intensity produced by one magnetic moment $\boldsymbol{m}$ on an arbitrary point P is

$$\boldsymbol{B} = -\frac{\mu_0}{4\pi}\nabla\frac{\boldsymbol{m}\cdot r}{\|r\|_2^3} \tag{33}$$

where r represents the vector pointing to P from the center point of magnetic moment, μ_0 is the permeability of vacuum.

The interacting magnetic force between two magnetic moments is obtained by solving the Maxwell equations with the introduction of a scalar magnetic potential $U_m = -\boldsymbol{B}\cdot\boldsymbol{m}_2$ (Yung *et al.*, 1998):

$$\begin{aligned}\boldsymbol{F} &= -\nabla U_m \\ &= -\frac{\mu_0}{4\pi}\nabla\left[\left(\nabla\frac{\boldsymbol{m}_1\cdot\boldsymbol{r}}{r^3}\right)\cdot\boldsymbol{m}_2\right]\end{aligned} \tag{34}$$

where m_1 and m_2 represent magnetic moments of two interacting magnetic dipoles.

For different shapes of permanent magnets, we just change the volume of magnet to calculate the interacting force (Stanton *et al.*, 2012; Neubauer *et al.*, 2012). Here taking cuboid magnets, for example, the related positions of two moments are parallel and opposite shown as Figure 14. Subsequently, the interacting magnetic force expression can be derived as:

$$\begin{aligned}\boldsymbol{F} &= \nabla(\boldsymbol{m}\cdot\boldsymbol{B}) \\ &= -\frac{3\mu_0 m_A m_B}{4\pi r_{AB}^4}\left[\left(1-5\frac{z^2}{r_{AB}^2}\right)\frac{x}{r_{AB}}\boldsymbol{i} + \left(1-5\frac{z^2}{r_{AB}^2}\right)\frac{y}{r_{AB}}\boldsymbol{j} + \left(3\frac{z}{r_{AB}} - 5\frac{z^3}{r_{AB}^3}\right)\boldsymbol{k}\right],\end{aligned} \tag{35}$$

where $r_{AB} = (x^2 + y^2 + z^2)^{1/2}$, $m_A = M_A V_A$ and $m_B = M_B V_B$ are magnetic moment of two dipoles.

The volumes of cuboid, cylindrical and spherical magnets are expressed as $V = lhw$, $V = l\pi R^2$ and $V = \frac{4}{3}\pi R^3$.

3. Experimental verification

3.1 Experiment details

In order to verify the accuracies of the equivalent models in calculating the interaction between permanent magnets, it is necessary to design an experiment to measure the actual interaction between permanent magnets. Because the dual permanent magnet interaction system in several models is equivalent to the force of one permanent magnet (A) in the magnetic field generated by the other permanent magnet (B), the magnetic interacting force is

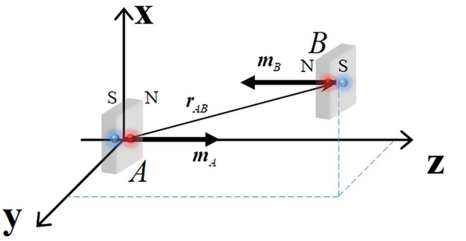

Figure 14.
Single magnetic dipole–dipole model describes interaction between cuboid permanent magnets

selected as the measurement object in this paper to verify the applicability of the equivalent models.

The experimental setup for static magnetic force measurement consists of a weight-bearing base, a 3D fine adjustment system, a dynamometer (HF-5) and a laser displacement sensor (LK-FG001V), as shown in Figure 15. One magnet of each pair is attached to the adjusted platform and the other one to the dynamometer. The like magnetic poles are arranged face to face, which means the axial repulsive magnetic forces exist between the magnet pairs in this experiment. We adjust the screws to simulate different relative positions of the magnets, while recording the displacements and forces in the laser displacement sensor and dynamometer, respectively, whose minimum resolutions are 0.001mm and 0.001N.

3.2 Measurement methods of interacting magnetic force

In order to conveniently and clearly compare the calculation accuracies of each equivalent model, two measurement modes are defined in this paper, namely two relative moving modes of permanent magnet pairs:

(1) Keep the interval between magnets constant, adjust to make one of the permanent magnets move along the x-axis, simultaneously measure the lateral and axial magnetic forces between two permanent magnets at different displacements. In this definition, the lateral magnetic direction is consistent with the moving direction of the permanent magnet, namely the x-axis direction. (Since the permanent magnets selected in this paper have square and circular pole surfaces, respectively, the same result will be obtained if the moving direction of the permanent magnets and the lateral force are defined as y-axis.) Besides, the displacement of the moving magnet is defined as zero when the projections of the pair of magnets coincide. Finally, the curves of axial and lateral magnetic forces with respect to lateral displacements between permanent magnets are achieved. This measurement mode is shown in Figure 16, where magnet B is a movable permanent magnet.

(2) The projection of two permanent magnets on the $x-y$ plane remains coincident, make one of them move along the z axis, that is, the interval between the two permanent magnets is changed. At this time, the lateral magnetic force between the permanent magnets is zero. Therefore, only the axial magnetic force in z-axis needs to be measured. Finally, the curves of axial force with respect to interval between permanent magnets are obtained. This measurement mode is shown in Figure 17.

4. Simulation and comparison

According to the expressions of interacting magnetic force achieved in the previous section, we use MATLAB to simulate the magnetic curves based on the two measurement modes described earlier. By comparing the measured data with the simulation results, the applicability and accuracies of different equivalent models can be verified and compared.

The cuboid permanent magnet is chosen as 10 mm $\times$ 10 mm $\times$ 2 mm N38H $Nd_2Fe_{14}B$ magnet. The cylindrical permanent magnet is chosen as ϕ6 mm $\times$ 2 mm N38H $Nd_2Fe_{14}B$ magnet. The spherical permanent magnet is chosen as ϕ30 mm Y30BH ferrite magnet. Simulation results comparing with experiment data of cuboid, cylindrical and spherical permanent magnet pair are shown in Figures 1–3, respectively.

It is worth noting that in the expressions of the interacting magnetic force between permanent magnets based on each aforementioned equivalent model, the magnetization

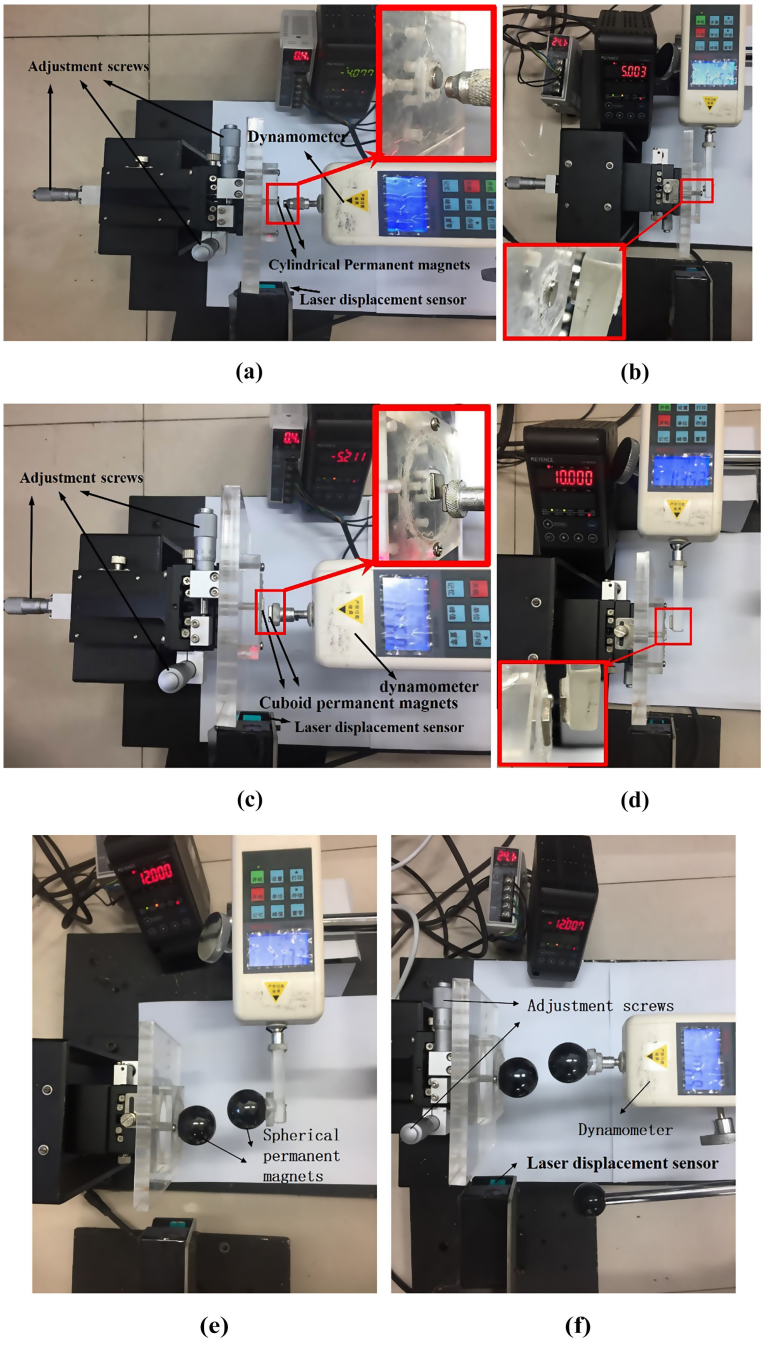

Figure 15.
Magnetic force measurement system. (a) axial force between cylindrical magnet pair, (b) lateral force between cylindrical magnet pair, (c) axial force between cuboid magnet pair, (d) lateral force between cuboid magnet pair, (e) lateral force between spherical magnet pair, (f) axial force between spherical magnet pair

intensity M does not participate in the integral, which means that the magnetization intensity M can be placed at the front or the last of the magnetic force expression as a coefficient for the permanent magnets uniformly magnetized. The general shape of the curve is not affected by the magnetization value of a single permanent magnet, except the magnitude of the entire curve, whether with mode 1 or mode 2.

Therefore, we assign the values of magnetization based on empirical criterions in the former researches and literatures to make the most of measured values consistent with the curves. Concretely, in this paper, by comparing the variance of the absolute error between the simulated value and the experimental data under different magnetization values:

$$Var = \frac{\sum_{i=1}^{N} (\Delta F_i)^2}{N}, \tag{36}$$

we confirm the final magnetization intensity's value when the variance is minimum. The ΔF_i in Eqn. (36) represents the absolute error of every force's value and is given by $\Delta F_i = F_{ei} - F_{si}(M)$, where F_{ei}, F_{si} and N represent the measured value, simulated value and the quantity of the values, which contains both axial and lateral forces of each equivalent model. The minimum variance means the best agreement between experiment and simulation with the achieved magnetization intensity. Finally, the magnetization value of cuboid, cylinder and spherical permanent magnets in the experiment in this paper is assigned when the interaction magnetic force is calculated based on different equivalent models, as shown in Table 1.

In order to compare the calculation accuracy of each equivalent model, this paper calculates the average relative error of each calculation model:

$$\overline{E}_r = \frac{\sum_{i=1}^{N} \left| \frac{\Delta F_i}{F_{ei}} \right|}{N}, \tag{37}$$

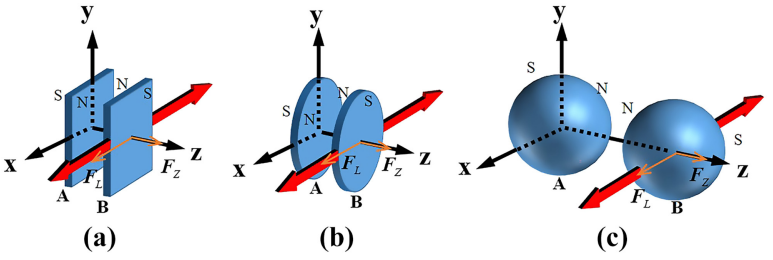

Figure 16.
Measurement mode 1. (a) Cuboid permanent magnets, (b) cylindrical permanent magnets, (c) spherical permanent magnets

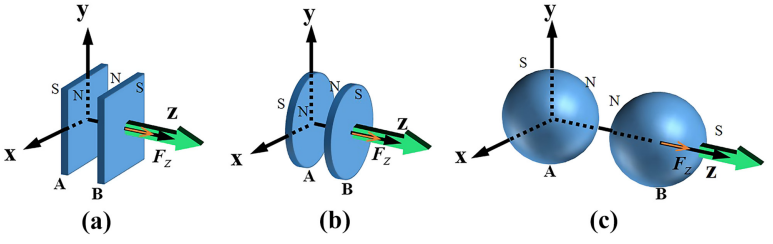

Figure 17.
Measurement mode 2. (a) Cuboid permanent magnets, (b) cylindrical permanent magnets, (c) spherical permanent magnets

excluding values of magnetic force smaller than 0.05N, which cannot be measured because of the zero-drift error of the dynamometer in the experiment. The average relative errors are shown and compared in Table 2.

By observing the analysis of Figures 18–20, as well as Table 2, we find that the equivalent magnetizing current model and the magnetic charge model have high accuracy in calculating the interacting magnetic force of cuboid, cylindrical and spherical permanent magnets. The equivalent magnetic dipole model only has a good advantage in describing spherical permanent magnets and is not applicable to the calculation of nonspherical permanent magnets.

Then, combining the data in Table 1 and Table 2, it can be found that for the same pair of permanent magnets, the equivalent models with similar good accuracies also have similar magnetization intensities. For example, for cuboid or cylindrical permanent magnets, the magnetization intensity of equivalent magnetizing current and magnetic charge model is similar. For spherical permanent magnets, magnetization intensities of equivalent magnetizing current, equivalent magnetic charge and equivalent magnetic dipole model are similar.

In conclusion, the equivalent magnetization current model and the equivalent magnetic charge model can be used to analyze the interaction of permanent magnets with any shape and have equivalence. Magnetic dipole is unable to describe the specific shape of the permanent magnet, just simply treating all magnets as a magnetic moment (Zhang *et al.*, 2017b). However, because dipole as a dot can be treated as a sphere in topology, magnetic dipole model can be only applied to calculation and analysis about spherical permanent magnet.

5. Conclusion

Taking magnet pairs of three kinds of typical shapes for examples as calculation objects, this paper detailedly demonstrates the procedures of interacting magnetic force calculations between permanent magnets with three popular equivalent models, magnetizing current model, magnetic charge model and magnetic dipole–dipole model. It is affirmed that the equivalent magnetizing current model and magnetic charge model have similar high accuracy and have equivalence when describing all three kinds of magnets, cuboid,

Table 1.
Magnetization values of different-shape permanent magnets based on each model

	Magnetizing current	Magnetic charge	Magnetic dipole
Cuboid magnet	5.72×10^5	5.85×10^5	1.89×10^5
Cylindrical magnet	7.97×10^5	8.09×10^5	4.20×10^5
Spherical manget	2.77×10^5	2.91×10^5	2.83×10^5

Table 2.
Average relative errors of each models for different-shape permanent magnets

	Magnetizing current	Magnetic charge	Magnetic dipole
Cuboid magnet	6.34%	5.22%	75.94%
Cylindrical magnet	2.48%	1.52%	44.49%
Spherical magnet	7.09%	9.10%	9.93%

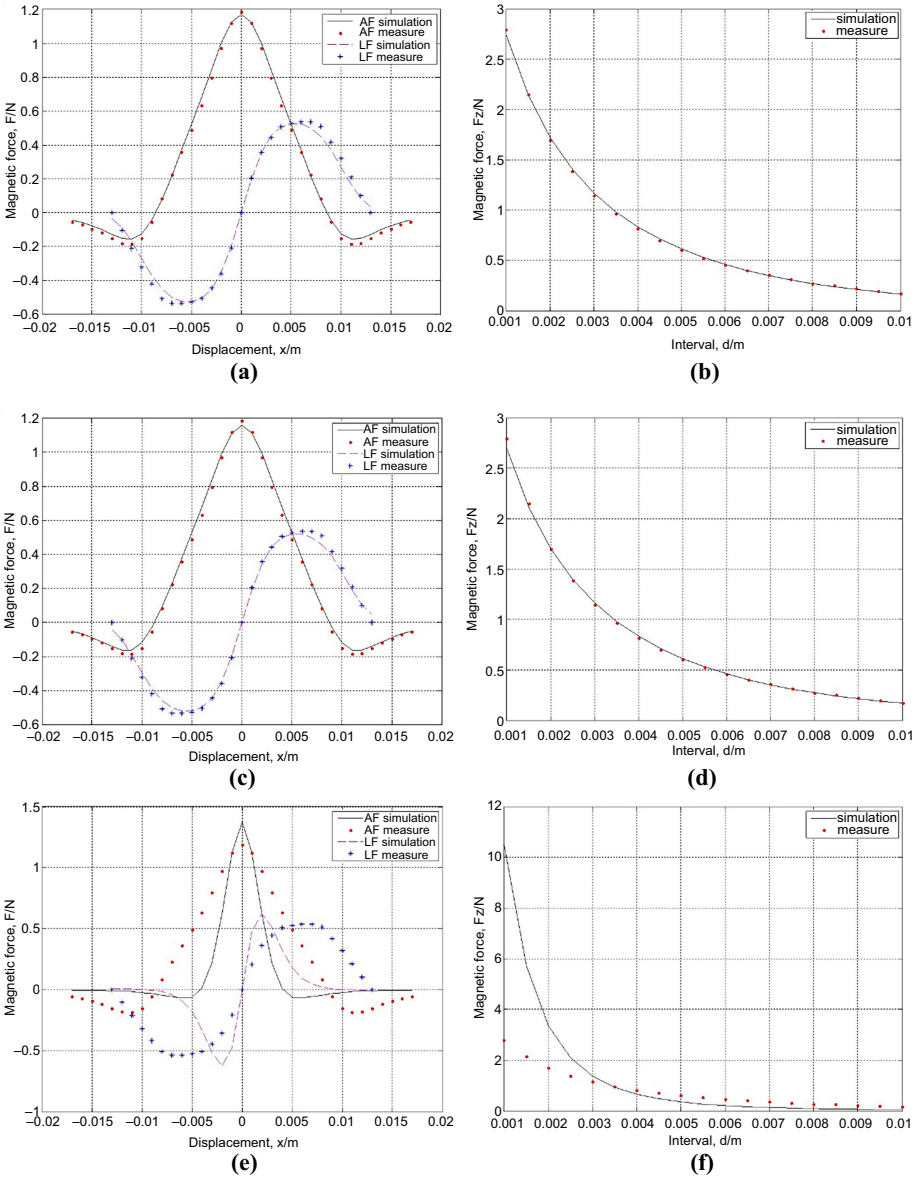

Figure 18. Comparison of simulation results based on (a)–(b) magnetizing current model, (c)–(d) magnetic charge model and (e)–(f) magnetic dipole–dipole model with the experiment data, for interacting magnetic force between cuboid permanent magnets

cylindrical and spherical permanent magnets. However, magnetic dipole–dipole model is only appropriate for spherical permanent magnet instead of the cubic or cylindrical magnet, because dipole model cannot describe the specific shape of permanent magnet, only sphere is the topological form of a dipole as a filled dot. Lots of applications could refer to our work, which is valuable for choosing the most appropriate model to solve the problems on magnetic force calculation based on permanent magnets with different kinds of shapes.

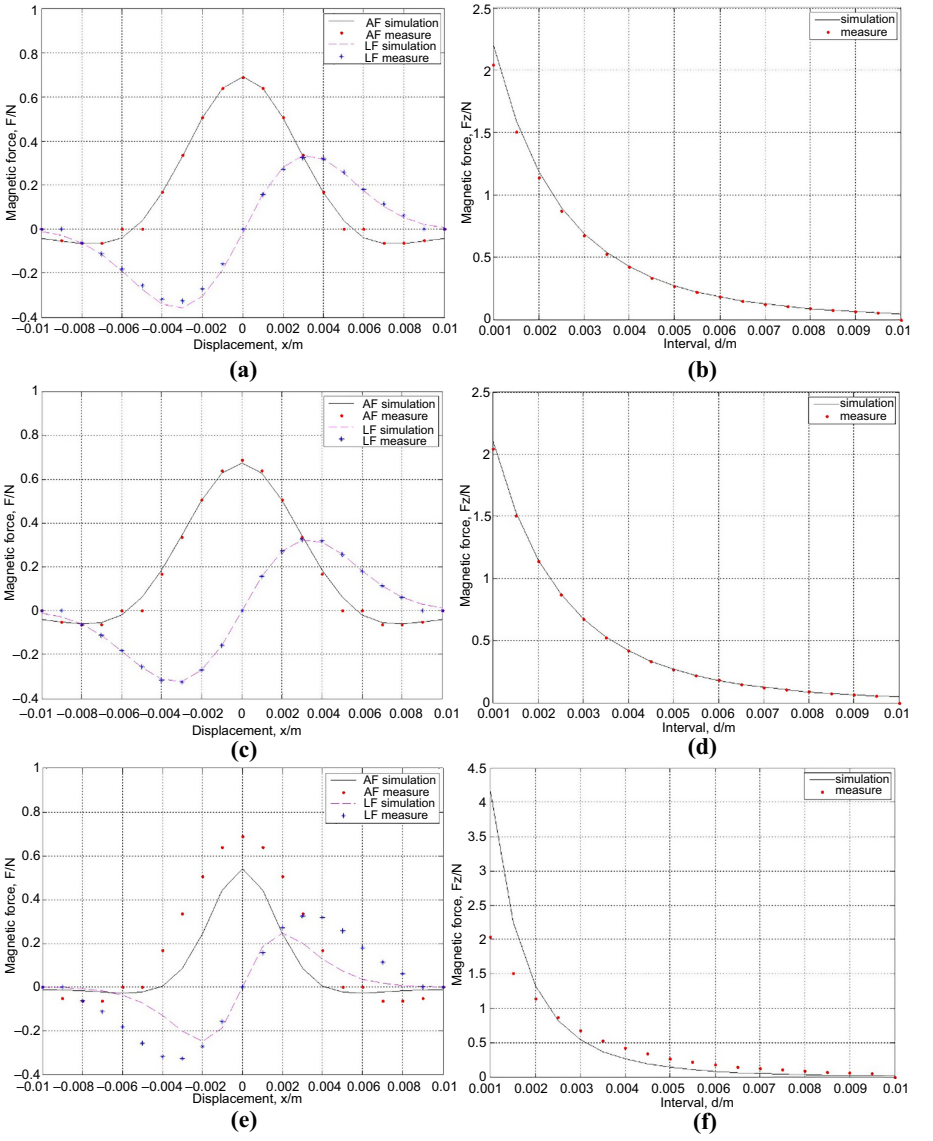

Figure 19.
Comparison of simulation results based on (a)–(b) magnetizing current model, (c)–(d) magnetic charge model and (e)–(f) magnetic dipole–dipole model with the experiment data, for interacting magnetic force between cylindrical permanent magnets

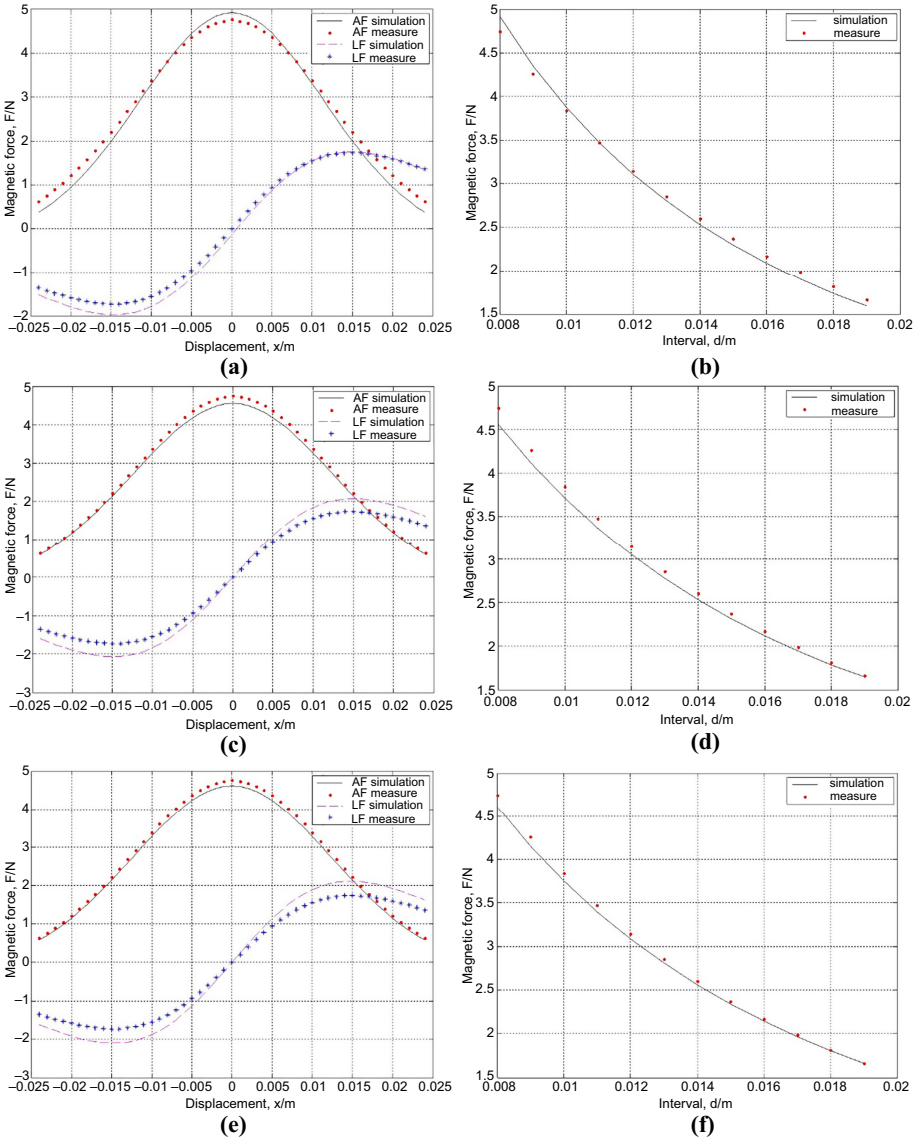

Figure 20.
Comparison of simulation results based on (a)–(b) magnetizing current model, (c)–(d) magnetic charge model and (e)–(f) magnetic dipole–dipole model with the experiment data, for interacting magnetic force between spherical permanent magnets

References

Agashe, J.S. and Arnold, D.P. (2008), "A study of scaling and geometry effects on the forces between cuboidal and cylindrical magnets using analytical force solutions", *Journal of Physics D Applied Physics*, Vol. 41 No. 10, p. 105001.

Bobbio, S. and Delfino, F. (2000), "Equivalent sources methods for the numerical evaluation of magnetic force with extension to nonlinear materials", *IEEE Transactions on Magnetics*, Vol. 36 No. 4, pp. 663-666.

Choi, H.S., Park, I.H. and Lee, S.H. (2006), "Concept of virtual air gap and its applications for force calculation", *IEEE Transactions on Magnetics*, Vol. 42 No. 4, pp. 663-666.

Gysen, B.L.J., Meessen, K.J., Paulides, J.J.H. and Lomonova, E.A. (2009), "General formulation of the electromagnetic field distribution in machines and devices using fourier analysis", *IEEE Transactions on Magnetics*, Vol. 46 No. 1, pp. 39-52.

Hutterer, M. and Gerald, K.M.S. (2017), "Redundant unbalance compensation of an active magnetic bearing system", *Mechanical Systems and Signal Processing*, Vol. 94 No. SEP, pp. 267-278.

Janssen, J.L.G., Paulides, J.J.H., Compter, J.C. and Lomonova, E.A. (2010), "Three-dimensional analytical calculation of the torque between permanent magnets in magnetic bearings", *IEEE Transactions on Magnetics*, Vol. 46 No. 6, pp. 1748-1751.

Kim, C.W. and Choi, J.Y. (2016), "Parametric analysis of tubular-type linear magnetic couplings with Halbach array magnetized permanent magnet by using analytical force calculation", *Journal of Magnetics*, Vol. 21 No. 1, pp. 110-114.

Kim, J.M., Choi, J.Y., Koo, M.M., Shin, H.J. and Lee, S.H. (2016), "Characteristic analysis of tubular-type permanent-magnet linear magnetic coupling based on analytical magnetic field calculations", *IEEE Transactions on Applied Superconductivity*, Vol. 26 No. 4, pp. 1-5.

Li, J. (2015), *Research on the Force and Torque between Permanent Magnets*, Ph.D. thesis, Jilin University, Changchun.

Li, J. (2018), "Interaction forces and torques between two perpendicular magnetic tubes", *Journal of Magnetics*, Vol. 23 No. 1, pp. 35-40.

Liang, P., Chai, F., Bi, Y., Pei, Y. and Cheng S. (2016), "Analytical model and design of spoke-type permanent-magnet machines accounting for saturation and nonlinearity of magnetic bridges", *Journal of Magnetism and Magnetic Materials*, Vol. 417 No. nov, pp. 389-396.

Liu, Z.J., Li, J.T. and Jabbar, M.A. (2006), "Prediction and analysis of magnetic forces in permanent magnet brushless dc motor with rotor eccentricity", *Journal of Applied Physics*, Vol. 99 No. 8Pt3, pp. 5157-5159.

Liu, P., Wang, Y. and Wu, J. (2009), "Design and fabrication of magnetic couplings in vacuum robots", *Industrial Robot-The International Journal of Robotics Research and Application*, Vol. 36 No. 3, pp. 230-237.

Neubauer, M., Twiefel, J., Westermann, H. and Wallaschek, J. (2012), "Modeling aspects of nonlinear energy harvesting for increased bandwidth", *Small-Scale Energy Harvesting, IntechOpen*, chapter 13, pp. 303-326.

Sadowski, N., Lefèvre, Y., Lajoie-Mazenc, M. and Bastos, J.P.A. (1992), "Sur le calcul des forces magnétiques", *Journal de Physique III*, Vol. 2, pp. 859-870.

Stanton, S.C., McGehee, C.C. and Mann, B.P. (2012), "Nonlinear dynamics for broadband energy harvesting: investigation of a bistable piezoelectric inertial generator", *Physica D: Nonlinear Phenomena*, Vol. 239 No. 10, pp. 640-653.

Sun, J., Wang, C. and Le, Y. (2016), "Designing and experimental verification of the axial hybrid magnetic bearing to stabilization of a magnetically suspended inertially stabilized platform", *IEEE/ASME Transactions on Mechatronics*, Vol. 21 No. 6, pp. 2881-2891.

Teyber, R., Trevizoli, P.V., Christiaanse, T.V., Govindappa, P., Niknia, I. and Rowe, A.M. (2017), "Permanent magnet design for magnetic heat pumps using total cost minimization", *Journal of Magnetism and Magnetic Materials*, Vol. 442, pp. 87-96.

Wang, Y. (2007). "Introduction", *Analysis and Design Methods of Magnetic Machine*, Hefei University of Technology press, pp. 2-20.

Wang, Y., Zhang, S. and Chen, G. (2012), "A novel continuously adjustable magnetic-valve controllable reactor and its modeling", *Proceedings of The 7th International Power Electronics and Motion Control Conference*, Harbin.

Yung, K.W., Landecke, P.B. and Villani, D.D. (1998), "An analytic solution for the force between two magnetic dipoles", *Magnetic and Electrical Separation*, Vol. 9 No. 1, pp. 39-52.

Zan, H. (2008), *Research on Demagnetizing Field Theory of Magnetic Materials*, M. S. thesis, Xi'an University of Architecture and Technology, Xi'an.

Zhang, Y., Leng, Y., Tan, D., Liu, J. and Fan, S. (2017), "Accurate analysis of magnetic force of bi-stable cantilever vibration energy harvesting system with the theory of magnetizing current", *Acta Physica Sinica*, Vol. 66 No. 22, p. 220502.

Zhang, Y., Leng, Y. and Fan, S. (2017), "The accurate analysis of magnetic force of bi-stable piezoelectric cantilever energy harvester", *Proceeding of International Design Engineering Technical Conferences and Computers and Information in Engineering Conference ASME*, Cleveland.

Zhao, K. and Chen, X. (2011), *Electromagnetism*, 3rd ed., Higher Education Press, Beijing, pp. 382-401.

Zhao, H. (2003), "Review on study on magnet machine and mechanism", *Chinese Journal of Mechanical Engineering*, Vol. 39 No. 12, pp. 31-36.

Zhao, J., Gao, R., Chen, G., Liu, S., Cao, Q. and Tao, Q. (2015), "Nonlinear coupling mechanical model for large stroke magnetic-based multistable mechanisms", *Mechanism and Machine Theory*, Vol. 83, pp. 56-68.

Corresponding author
Yonggang Leng can be contacted at: leng_yg@tju.edu.cn